Characterization of dynamic recrystallisation in as-homogenized Mg–Zn–Y–Zr alloy using processing map

Y. WANG, Y. ZHANG*, X. ZENG, W. DING
National Engineering Research Center of Light Alloys Net Forming, Shanghai Jiao Tong University, 1954 Huashan Road, 200030 Shanghai, People Republic of China

Published online: 21 April 2006

The hot working behavior of a as-homogenized Mg–Zn–Y–Zr alloy has been investigated in the temperature range 200–400°C and strain rate range 0.0015–7.5 s^{-1} using processing map. The power dissipation map reveals that a domain of dynamic recrystallisation (DRX) in the temperature range 300–400°C and strain rate range 0.0015–0.15 s^{-1}, with its peak efficiency of 38% at 350°C and 0.0015 s^{-1}, which are the optimum hot working parameters. The apparent activation energy in the hot deformation process is 148 ± 3 KJ/mol that is larger than that of ZK60 alloy because of the obstruction of Y atoms for diffusion. DRX model indicates that DRX of Mg–Zn–Y–Zr alloy is controlled by the rate of nucleation, which is lower one order of magnitude than growth. And the rate of nucleation depends on the process of mechanical recovery by cross-slip of screw dislocations.

1. Introduction

Magnesium and its alloys have been perceived to have poor ductility and poor cold workability at ambient temperature because of its highly anisotropic dislocation slip behavior. The critical resolved shear stresses (CRSS) of a basal slip system at room temperature is approximately 1/100 those of non-basal slip systems on prismatic and pyramidal planes. Whereas, the basal slip system can only provides two independent slip systems, far fewer than the necessary five independent systems for homogeneous deformation [1]. However, the CRSS of non-basal slip systems drops rapidly with increasing temperature which is in favor of improving deformability of magnesium and its alloys at elevated temperature [2]. Wrought Mg–Zn–Y–Zr alloys attracted significant interest because they have both high strength at both room and elevated temperatures [3]. But the attention is paid to the phase transformations in these wrought alloys [4–7], and few attentions to its deformability [8]. The aim of the present investigation is to develop a processing map with a view to understanding its characterization of dynamic recrystallisation (DRX) and optimizing its hot workability. The processing map is developed on the basis of dynamic materials model (DMM) [9]. In this model, the workpiece under hot working conditions is considered to be a dissipater of power. At any moment the total power dissipation consists of two complementary parts, the G content represents the temperature increase and J co-content represents the dissipation through metallurgical process, that is, the total power dissipation P:

$$P = \sigma \cdot \dot{\varepsilon} = G + J = \int_0^{\dot{\varepsilon}} \sigma d\dot{\varepsilon} + \int_0^{\sigma} \dot{\varepsilon} d\sigma \qquad (1)$$

And it is found that strain rate sensitivity of flow stress m is given by:

$$m = dJ/dG = \dot{\varepsilon} d\sigma/\sigma d\dot{\varepsilon} = \dot{\varepsilon}\sigma d\ln\sigma/\sigma\dot{\varepsilon} d\ln\dot{\varepsilon} \approx \Delta\log\sigma/\Delta\log\dot{\varepsilon} \qquad (2)$$

After integrated, the J co-content can be given by:

$$J = \sigma\dot{\varepsilon}m/(m+1) \qquad (3)$$

where σ is the flow stress and $\dot{\varepsilon}$ is the strain rate. In the "kinetic" constitutive Equation, m varies with strain rate and is nonlinear which leads to the J co-content nonlinear. For an ideal linear dissipation, $m = 1$ and $J = J_{max} = \sigma\dot{\varepsilon}/2$. Therefore, efficiency of power dissipation of a nonlinear

*Author to whom all correspondence should be addressed.
0022-2461
DOI: 10.1007/s10853-005-5564-x

dissipater can be expressed as a dimensional parameter,

$$\eta = J/J_{\max} = 2m/(m+1) \quad (4)$$

η represents the power dissipation characteristics occurring through metallurgical changes in the workpiece material and constitutes a processing map with temperature and strain rate. This methodology has been used to optimize hot workability of various materials, such as Zr [10], ETP copper [11], as-cast magnesium [12] and as-cast [13] and hot-rolled [14] Mg-11.5Li-1.5Al alloy etc. successfully.

2. Experimental

Mg–Zn–Y–Zr (Zn, 5.55 wt%; Y, 1.72 wt%; Zr, 0.37 wt%; Mg, Bal.) alloy was melted in a mild steel crucible with the protection of a mixed gas atmosphere of SF_6 (1 vol.%) and CO_2 (99 vol.%). When the temperature reached 750°C, molten metal was stirred for about 5 min, and then poured into a steel mold with diameter of 45 mm and height of 100 mm preheated to 200°C. The initial grain size is about 45 μm.

Cylindrical specimens of 10 mm diameter and 15 mm height were machined from the ingot homogenized at 400°C for 18 h and used for compression testing. Hot compression test was performed on Gleebe-3000 simulator in a temperature range of 200–400°C at intervals of 50°C and in the strain rate range of 1.5×10^{-3}–7.5 s^{-1}. In each test, the specimens were compressed to about half their original height and the load-displacement data were obtained and corrected. The procedure for obtaining the power dissipation maps was conducted following that mentioned in [9].

3. Results

True stress-true strain curves are shown in Fig. 1a–c at 200, 300 and 400°C respectively, for various strain rates. The curves at other temperatures are similar to those in Fig. 1. At strain rates above 0.015 s^{-1}, the curves exhibit flow softening, whereas other curves show steady state behavior for the temperature below 250°C. However, for the temperature above 250°C, the curves exhibit flow softening at strain rates above 0.15 s^{-1}, and other curves show steady state behavior. Fig. 2 shows relationship between peak strain and temperature at different strain rates. It can be found that the peak strain decrease with the increasing of temperature and decreasing of strain rates.

Power dissipation maps at strains of 0.1, 0.3 and 0.5 are shown in Fig. 3. The strain of 0.1 is considered to represent strains below the critical strain for all strain rates, the strain of 0.3 indicates those close to the critical strain and the strain of 0.5 corresponds to those at the steady state for most of the strain rates. The maps at other

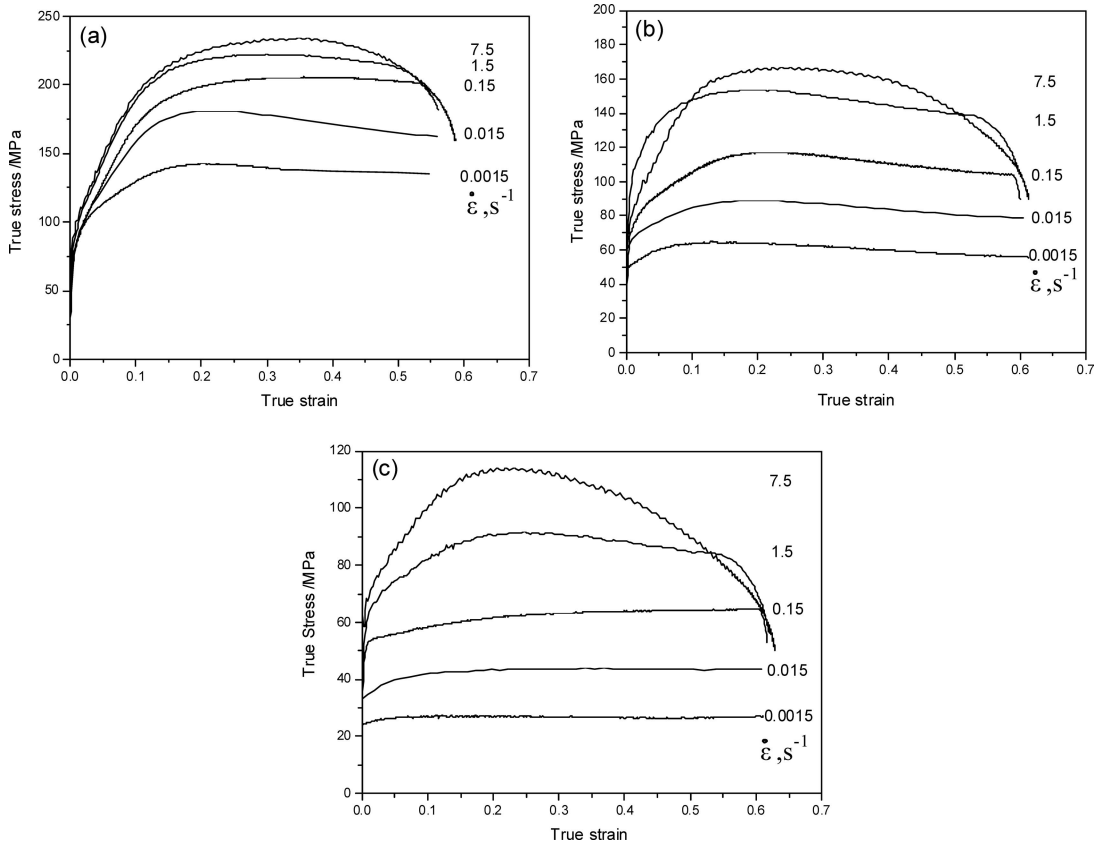

Figure 1 True stress-true strain cures obtained at (a) 200°C, (b) 300°C and (c) 400°C at various strain rates.

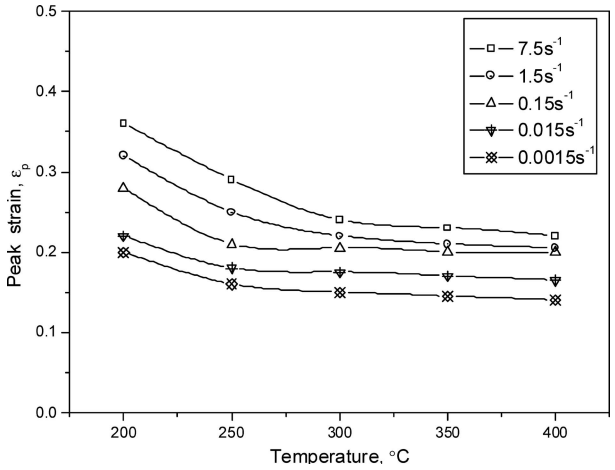

Figure 2 Variation of peak strain with temperature at various strain rates.

strains are similar to those in Fig. 3 which shows that there is no effect of strain on the power dissipation maps. These maps show a single domain in the temperature range 300–400°C and strain rate range 0.0015–0.15 s^{-1}, with a peak efficiency of about 38% occurring at about 350°C and 0.0015 s^{-1}. The domain changes narrow with increasing strains toward lower strain rate.

4. Discussion

4.1. Dynamic recrystallisation

According to the interpretation of DRX domain in processing map, the efficiency of power dissipation is 30–40% in the low stacking fault energy (SFE) materials. The SFE of magnesium is reported [12] to be about 60–78 mJm^{-2} belonging to low SFE materials. The efficiency is about 34% for as-cast magnesium [12] whose DRX domain occurring at 425°C and 0.3 s^{-1}. That for Mg-2Zn-1 Mn [15] alloy is about 33%, its DRX domain occurring at 450°C and 0.1 s^{-1}. Therefore, the domain occurring at 350°C and 0.0015 s^{-1} may be interpreted as a DRX domain. Microstructure of a sample deformed in this domain is shown in Fig. 4. DRX occurs completely. The efficiency of power dissipation and average grain size vs. temperature are shown in Fig. 5 corresponding to the strain rate of 0.0015 s^{-1}. The grain size increases with temperature and shows a sigmoid. The temperature at which a 50% change in grain size has occurred is termed as DRX temperature

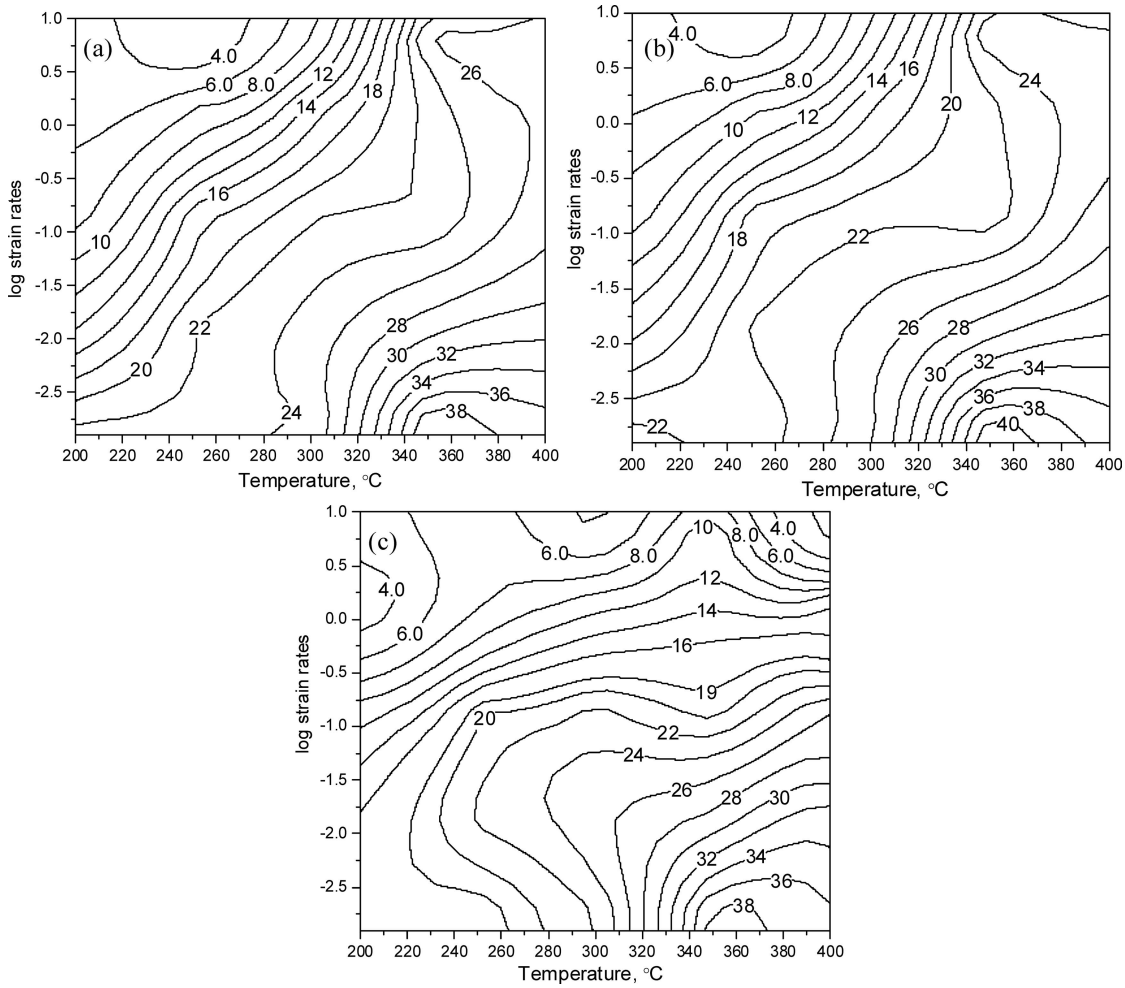

Figure 3 Power dissipation maps obtained at strains of (a) 0.1, (b) 0.3 and (c) 0.5. (Numbers on contours represent isoefficiency (%) of power dissipation).

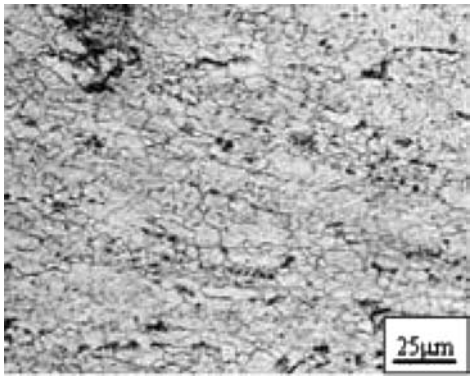

Figure 4 Microstructure in DRX domain at 350°C and 0.0015 s^{-1}.

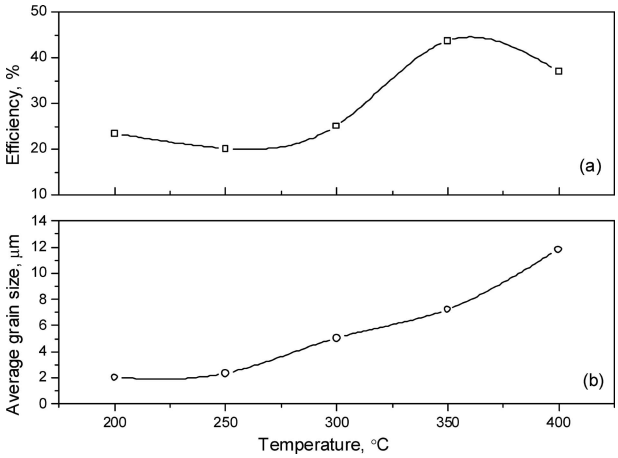

Figure 5 Variation of (a) efficiency of power dissipation and (b) average grain size with temperature at the strain rate of 0.0015 s^{-1}.

[16] which is 350°C in Fig. 5. A comparison of the variations of grain size and efficiency at the strain rate of 0.0015 s^{-1} reveal that the DRX temperature corresponding to a 50% change in the grain size coincides with temperature for peak efficiency. Therefore, the peak efficiency in processing map represents the DRX temperature. The optimum parameters for hot working of this material are 350°C and 0.0015 s^{-1}. The DRX formation mechanism is discontinuous dynamic recrystallisation (DDRX) that is controlled by high-temperature dislocations climb in pure magnesium [12], Mg-2Zn-1 Mn [15] and AZ31 [17] alloy. Hence, the DRX temperature of these magnesium alloys is higher. However, the DRX formation mechanism of Mg–Zn–Y–Zr alloy is continuous dynamic recrystallisation (CDRX) which is controlled by cross-slip in the intermediate temperature. High temperature will lead to the increasing DRX grain size and lower dissipation efficiency (discussed in Section 4.3). Therefore, the optimum DRX temperature of Mg–Zn–Y–Zr alloy is lower than that of other magnesium alloys.

4.2. Kinetic analysis

In the kinetic analysis, the effects of temperature and strain rate on flow stress are expressed by the following Equation:

$$A(\sinh\alpha\sigma_p)^n = \dot{\varepsilon}\ \exp(Q/RT) = Z \qquad (5)$$

where A is a constant, n is stress exponent (= 1/m), α = 0.0052 MPa^{-1} [17], $\dot{\varepsilon}$ is strain rate, R is gas constant, T is absolute temperature, Q is activation energy and Z is the Zener-Hollomon parameter incorporating the two control variables T and $\dot{\varepsilon}$ through an Arrhenius function with activation energy Q. Then the activation energy Q can be expressed as:

$$Q = R\left[\frac{\partial \ln(\sinh \alpha\sigma)}{\partial {}^{1}\!/_{T}}\right]_{\dot{\varepsilon}}\left[\frac{\partial \ln \dot{\varepsilon}}{\partial \ln(\sinh \alpha\sigma)}\right]_{T} \qquad (6)$$

In order to calculate Q, stress exponent n is obtained from the ln $\dot{\varepsilon}$ vs ln(sinh$\alpha\sigma$) plots (Fig. 6)a and slope s is obtained from the ln(sinh$\alpha\sigma$) vs 1/T plots (Fig. 6b). The mean activation energy Q (ns$R$) is calculated to be 148 ± 3 KJ/mol and larger than 140 KJ/mol for ZK60 alloy [18] which results from the Y solute atoms hampering the lattice diffusion of Mg. The plot including Z brings all test data into a single line which confirms the fit with a correlation coefficient r = 0.982 (Fig. 6c).

4.3. Mechanism of dynamic recrystallisation

DRX is the phenomenon by which the stored energy present in a deforming microstructure is used to generate new, dislocation free, grains during the deformation process [19]. It consists of two occurring simultaneously and competing processes-nucleation (formation of interfaces) and growth (migration of interfaces) which corresponding to two parallel processes-strengthening and softening. Strengthening results from the increasing of dislocation density due to dislocation generation. Meanwhile, dislocation rearrangement produce high angle boundary that forms a subgrain (nucleation). Softening results from the dislocation annihilation and incorporation (growth). A steady state is obtained when the dynamic balance of quantities of dislocation formation and dislocation annihilation. Therefore, the steady state reflects a dynamic balance between nucleation and growth, and between strengthening and softening. A. Galiyev *et al*. [20] investigate the deformation mechanism of ZK60 alloy, which demonstrates that at temperature range of 473 to 723 K, cross-slip and high-temperature dislocations climb are identified as controlling mechanisms for large-strain plastic flow in ZK60 magnesium alloy, that is, the controlling mechanism of plastic deformation is cross-slip of **a** dislocations (screw dislocations) on non-basal planes that results in the CDRX and the activation energy of plastic flow approaches the activation energy for volume self-diffusion, i.e., the controlling process is dislocation climb that brings on the DDRX. Mg–Zn–Y–Zr alloy investigated in this paper is a ZK60 alloy adding Y element, and

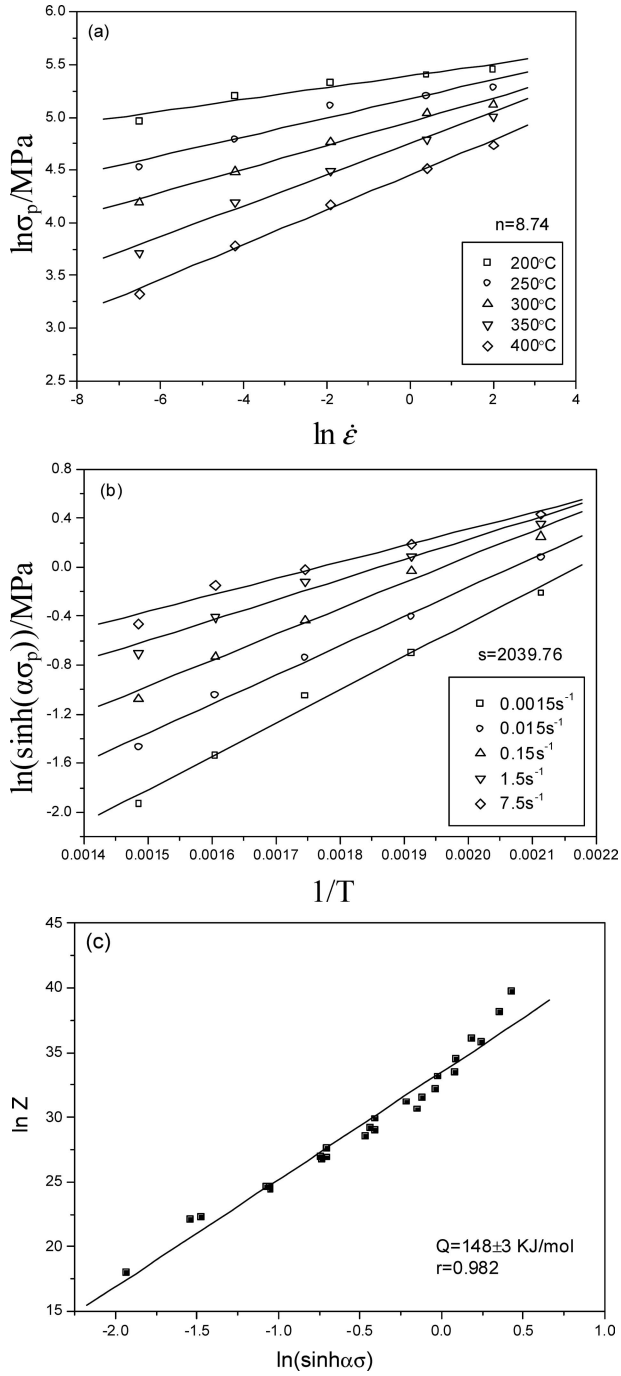

Figure 6 The dependence of peak strength on (a) strain rate, (b) temperature and (c) Z according to Equation 5.

therefore, the controlling mechanism for plastic deformation is same to that of ZK60 alloy.

DRX model proposed by Y.V.R.K. Prasad [16] is based on the nucleation and the rate of grain boundary migration, which are the two competing processes under a given constant true strain rate and the slower of the two rate controls DRX.

The rate of interface formation R_F depends on the rate of recovered dislocations generation

$$R_F = \dot{\varepsilon} P_R / b1 \tag{7}$$

where P_R is the probability of recovery of dislocations, b is the Burgers vector, and l is the dislocation link length (about 3×10^{-6} m). For mechanical recovery involving cross-slip of screw dislocations

$$P_R = \exp\{-\alpha G b^2 d[\ln(d/b)]^{1/2}/kT\} \tag{8}$$

where α is a constant (0.06), G is the shear modulus, d is the stacking fault width, k is the Boltzmann constant, and T is the DRX temperature.

The stacking fault width of magnesium is about 2b. Substituting $G = 1.75 \times 10^4$ MN m^{-2}, $b = 3.21 \times 10^{-10}$ m, and $d = 2$b, the probability of recovery by cross-slip in the tested alloy at the DRX temperature is about 1.2×10^{-3}.

For thermal recovery involving climb of edge dislocations

$$P_R = \exp(-Q/RT) \tag{9}$$

where Q is the activation energy. Substituting $Q_{SD} = 135$ kJ mol^{-1} [21], the probability of recovery by climb is about 4.8×10^{-12}.

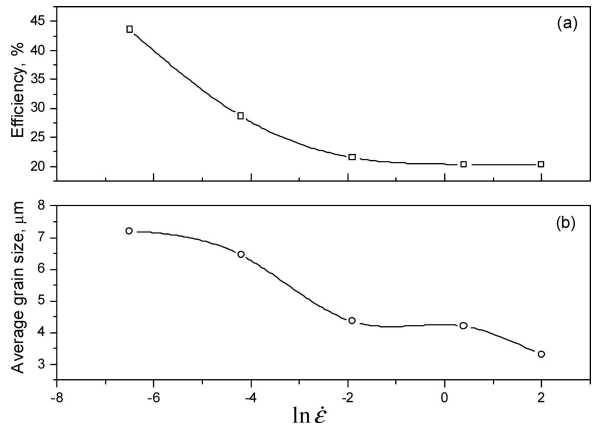

Figure 7 Variation of (a) efficiency of power dissipation and (b) average grain size with ln $\dot{\varepsilon}$ at 350°C and a strain of 0.5.

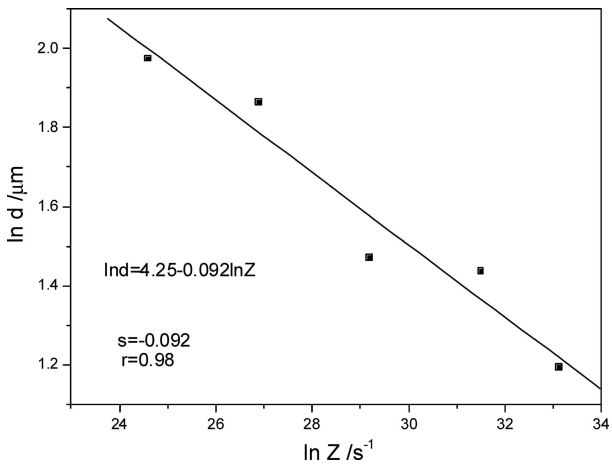

Figure 8 Variation of lnd (average grain size) with lnZ at 350°C and strain of 0.5.

Comparison of the probability of recovery by cross-slip and by climb reveals that recovery by cross-slip is about nine orders of magnitude faster than that by climb, hence, will control the rate of interface formation, which is then given by

$$R_F = (\dot{\varepsilon}/bl)\exp\{-\alpha Gb^2 d[\ln(d/b)]^{1/2}/kT\} \quad (10)$$

The DRX parameters in the investigated alloy are $\dot{\varepsilon} = 1.5 \times 10^{-3}\ s^{-1}$ and $T = 350°C$ and therefore $R_F = 1.9 \times 10^9\ m^{-2}\ s^{-1}$.

During the deformation of the Mg–Zn–Y–Zr alloy, dispersive precipitates [8] pinning the grain boundaries that leads to the suppression of formation for bulges of grain boundaries which results in nucleation of DDRX grains, and meanwhile, restricting the dislocation climb results in the formation of low-angle boundaries. Continuous absorption of dislocations in the low-angle boundaries results in CDRX. Hence, it is not high-temperature dislocations climb, but cross-slip of a dislocations that controls the nucleation of CDRX which can be proved by the above calculation.

The rate of interface migration of high angle grain boundaries R_M depends upon the grain boundary mobility M:

$$R_M = cM \quad (11)$$

$$M = D\Gamma/kTb \quad (12)$$

where D is the diffusion coefficient, Γ is the interfacial energy and c is a constant (about $10^{-3}\ m^{-1}$). Substituting $D = 4.8 \times 10^{-16}\ m^2\ s^{-1}$ at 350°C and $\Gamma = 340\ mJ\ m^{-2}$, then $R_M \approx 6 \times 10^{10}\ m^{-2}\ s^{-1}$ is obtained.

Hence, the rate of interface formation R_F is lower one order of magnitude than the rate of interface migration R_M and then controls the DRX process.

Combination the true stress-true strain curves (Fig. 1) with power dissipation maps (Fig. 3), it is found obviously that single peak stress-strain behavior appears in the DRX domain, whereas drooping [16] stress-strain behavior occurs outside the DRX domain. At lower strain rates ($0.0015\ s^{-1}$), the rate of interface migration increases to be about 3.8×10^{11} at high temperature (400°C) owing to the rapid diffusion. The difference between R_F and R_M increases and the interface migration will consume some of the nuclei of DRX, making the process less efficient and increasing the DRX grain size (Fig. 5b). At strain rates higher than the DRX strain rate, time for interface migration is less and DRX is incomplete which results in the drooping stress-strain curves. At lower temperature, the rate of interface migration is lower (at constant strain rate), and at higher strain rate, the rate of interface formation is higher (at constant temperature), which also leads to the process less efficient and decreasing the DRX grain size (Fig. 5b and 7b). It is well known [22] that the grain size variation under DRX conditions may be correlated with the temperature compensated strain rate parameter (Zener-Hollomon) Z. The average grain size is plotted against Z on ln-ln scale in Fig. 8 when the specimens were deformed at DRX temperature. The plot exhibits a linear relationship, which can be expressed by the following equation:

$$\ln d = 4.25 - 0.092 \ln Z \quad (13)$$

References

1. J. KOIKE, T. KOBAYASHI, T. MUKAI, H. WATANABE, M. SUZUKI, K. MARUYAMA and K. HIGASHI, *Acta Materilia.* **51** (2003) 2055.
2. M. R. BARNETT, Z. KESHAVARZ, A. G. BEER and D. ATWELL, *ibid.* **52** (2004) 5093.
3. A. SINGH and A. P. TSAI, *Scripta Materialia.* **49** (2003) 143.
4. E. M. PADEZHNOVA, E. V. MEL'NIK, R. A. MILIYEVSKIY, T. V. DOBATKINA and V. V. KINZHIBAO, *Russ. Metall. (Metally)* **4** (1982) 185.
5. Z. P. LUO and S. Q. ZHANG, *J. Mater. Sci. Lett.* **12** (1993) 1490.
6. W. F. SMITH (Ed.), in "Structure and Properties of Engineering Alloys", (McGraw-Hill, New York, 1993) p. 542.
7. F. S. PIERCE, S. J. POON and Q. GUO, *Science* **261** (1993) 737.
8. Y. ZHANG, X. Q. ZENG, L. F. LIU, C. LU, H. T. ZHOU, Q. LI and Y. P. ZHU, *Mater. Sci. Engng. A* **373** (2004) 320.
9. Y. V. R. K. PRASAD and S. SASIDHARA, "Hot working Guide: A compendium of processing maps", (ASM International Materials Park, OH, 1997).
10. J. K. CHAKRAVARTY, Y. V. R. K. PRASAD and M. K. ASUNDI, *Metall. Trans. A* **22** (1991) 829.
11. Y. V. R. K. PRASAD and K. P. RAO, *Mater. Sci. Engi. A* **374** (2004) 335.
12. O. SIVAKESAVAM, I. S. RAO and Y. V. R. K. PRASAD, *Mater. Sci. Technol.* **9** (1993) 805.
13. O. SIVAKESAVAM and Y. V. R. K. PRASAD, *Mater. Sci. Engi. A* **323** (2002) 270.
14. *Idem., Z. Metallkd.* **93** (2002) 123.
15. *Idem., Mater. Sci. Engi. A* **362** (2003) 118.
16. N. SRINIVASAN and Y. V. R. K. PRASAD, *Mater. Sci. Technol.* **8** (1992) 206.
17. A. MWEMBELA, E. B. KONOPLEVA and H. J. MCQUEEN, *Scripta Mater.* **37** (1997) 1789.
18. H. J. MCQUEEN, M. M. MYSHLYAEV and A. MWEMBELA, *Canadian Metall. Quarterly* **42** (2003) 97.
19. B. DERBY, *Scripta Metall. Mater.* **27** (1992) 1581.
20. A. GALIYEV, R. KAIBYSHEV and G. GOTTSTEIN, *Acta Mater.* **49** (2001) 1199.
21. H. J. FROST and M. F. ASHBY, in "Deformation-mechanism maps: the plasticity and creep of metals and ceramics", (Pergamon, Oxford, 1982) p. 44.
22. T. SAKAI and J. J. JONAS. *Acta Metall.* **32** (1984) 189.

Received 28 February
and accepted 29 August 2005